Magnetic structure of $CuCrO_2$: a single crystal neutron diffraction study

2012 J. Phys.: Condens. Matter 24 016004

(http://iopscience.iop.org/0953-8984/24/1/016004)

J. Phys.: Condens. Matter **24** (2012) 016004 (8pp) doi:10.1088/0953-8984/24/1/016004

Magnetic structure of $CuCrO_2$: a single crystal neutron diffraction study

M Frontzek[1], G Ehlers[1], A Podlesnyak[1], H Cao[1], M Matsuda[1], O Zaharko[2], N Aliouane[2], S Barilo[3] and S V Shiryaev[3]

[1] Neutron Scattering Science Division, Oak Ridge National Laboratory, Oak Ridge, TN 37831, USA
[2] Laboratory for Neutron Scattering, Paul Scherrer Institute, CH-5232 Villigen, Switzerland
[3] Institute of Solid State and Semiconductor Physics, Minsk 220 072, Belarus

E-mail: frontzekmd@ornl.gov

Received 26 August 2011, in final form 15 November 2011
Published 8 December 2011
Online at stacks.iop.org/JPhysCM/24/016004

Abstract

This paper presents results of a recent study of multiferroic $CuCrO_2$ by means of single crystal neutron diffraction. This system has two close magnetic phase transitions at $T_N = 24.2$ K and $T_{mf} = 23.6$ K. The low temperature magnetic structure below T_{mf} is unambiguously determined to be a fully three-dimensional proper screw. Between T_N and T_{mf} antiferromagnetic order is found that is essentially two-dimensional. In this narrow temperature range, magnetic near neighbor correlations are still long range in the (H, K) plane, whereas nearest neighbors along the L direction are uncorrelated. Thus, the multiferroic state is realized only in the low temperature three-dimensional state and not in the two-dimensional state.

(Some figures may appear in colour only in the online journal)

1. Introduction

Multiferroic materials have become of interest for their unusual low temperature properties in general, and in particular for the observation that one can affect their magnetic structure through an electric field and their electric polarization through a magnetic field. The most promising candidates for a controllable multiferroic have been found among the materials with inherent geometric magnetic frustration [1].

The magnetic properties of the delafossite $CuCrO_2$ have received detailed interest since the discovery of its multiferroic behavior [2–4]. This system, which crystallizes in the rhombohedral $R\bar{3}m$ space group, is a multiferroic compound due to its apparent strong coupling of spin and charge. In contrast to other multiferroic compounds $CuCrO_2$ shows a spontaneous electric polarization upon antiferromagnetic ordering without an accompanying structural phase transition, although a slight in-plane lattice distortion can be measured [5]. Further, $CuCrO_2$ is a rare example of a system whose magnetoelectric properties are tunable by both an electric and a magnetic field [3, 7]. Another particular property is that the multiferroic state is already entered in zero magnetic field as opposed to isostructural $CuFeO_2$ [10–12].

It should be noted that throughout this publication the crystal structure is described in the hexagonal setting. Several studies of the magnetic structure by neutron diffraction techniques with powder [13, 14] and single crystal [7, 15] samples have been reported. The powder experiments found an incommensurate magnetic propagation vector $\boldsymbol{\tau} = (0.329, 0.329, 0)$ based on the position of the $(0, 0, 0) + \boldsymbol{\tau}$ reflection, and a broadening of some of the magnetic Bragg peaks which was attributed to short range correlations along the L direction, either in the form of quasi-two-dimensionality [13] or as stacking faults [14]. The measured powder intensities were best described with a proper screw magnetic structure, although other magnetic structure models could not be unambiguously excluded. The single crystal experiments, on the other hand, identified the structure as an incommensurate proper screw but the magnetic moments were not refined, and, most importantly, measurements were only reported for $(H, K, 0)$ reflections [7, 15]. Thus the question of possible ordering along the L direction was not considered. In this contribution we will fill these gaps and

arrive at the following main conclusions. The low temperature magnetic structure below[4] T_{mf} is truly three-dimensional with long range correlations along the L direction. We confirm the incommensurate proper screw magnetic spiral propagating along the [1,1,0] direction, and find that it has an elliptical envelope with a modulation between $\mathbf{M}_{[1\bar{1}0]} = 2.2(2)\ \mu_B$ and $\mathbf{M}_{[001]} = 2.8(2)\ \mu_B$. Furthermore we characterize the spin structure in the intermediate temperature phase between T_N and T_{mf} (which is not multiferroic) as two-dimensional with a total lack of near neighbor magnetic correlations along the L direction.

2. Experimental details

Single crystal samples were prepared in two ways. Samples up to 6 mm^3 in size were grown in a platinum crucible by the high temperature solution technique based on the thermal decomposition of $K_2Cr_2O_7$ at 860 °C in the presence of CuO [16]. The mixture of $K_2Cr_2O_7$ (73 mol%) and CuO (27 mol%) was placed into a high density alumina crucible and heated quickly up to 850 °C. Then the temperature was lowered at a rate of 0.5 °C h^{-1} for a period of up to four days before the crucible was quenched to room temperature. This resulted in single crystalline black hexagonal platelets of up to 6 mm^3 in volume. Larger $CuCrO_2$ crystals (up to 60 mm^3) were grown with a flux melting technique based on Bi_2O_3 solvent at a temperature between 940 and 1250 °C, under conditions of repeating abrupt rise of temperature of 10–15 °C with subsequent cooling of 0.5–1.5 °C h^{-1}.

The trigonal crystal structure (space group $R\bar{3}m$, hexagonal axes) with room temperature lattice parameters $a = 2.976$ Å and $c = 17.110$ Å [17] was confirmed by x-ray powder analysis of crushed crystals. In this structure, the unmagnetic Cu^{1+}, the magnetic Cr^{3+} and the O^{2-} occupy the Wyckoff positions 3*a*, 3*b* and 6*c*, respectively [17]. Further characterization with respect to their magnetic properties was carried out using a SQUID magnetometer. The obtained susceptibility curves were similar to data published previously [2, 3, 14, 15]. Identifying the same characteristic points in the susceptibility data as Kimura *et al* [2], the same two characteristic phase transition temperatures, $T_N = 24.2$ K and $T_{mf} = 23.6$ K, were obtained for our samples.

Neutron single crystal diffraction experiments were performed on the TriCS four circle diffractometer at the SINQ facility, PSI, Switzerland, on the HB-1 triple axis spectrometer and the HB-3A four circle diffractometer (FCD) at HFIR at Oak Ridge National Laboratory (ORNL), and on the Cold Neutron Chopper Spectrometer (CNCS) at the Spallation Neutron Source (SNS) in Oak Ridge. The TriCS experiment used a single crystal of dimensions 3.5 mm × 3 mm × 1 mm mounted in two different orientations: with the [00*L*] direction (hexagonal setting) along the ϕ-shaft of the instrument (orientation 1) and with the $[\bar{H}H0]$ direction (orientation 2) along the ϕ-shaft. Orientation 1 gives good resolution in the H, K planes (L = const), while orientation 2 yields good resolution in the planes orthogonal to $[\bar{H}H0]$. For data collection in a broad **Q** range a neutron wavelength of $\lambda = 1.178$ Å (Ge-311 monochromator with vertical focusing [8]) was used without collimation between the sample and the ^{3}He single tube detector. For collecting maps and scans with high resolution a neutron wavelength of 2.32 Å was used (PG-002 monochromator, PG filter) with a 20′ collimation in front of the detector. The experiments on HB-3A FCD at HFIR used a single crystal of similar size, 3.2 mm × 2.5 mm × 1.0 mm, from the same batch. The crystal was mounted in the orientation 2. The neutron wavelength was $\lambda = 1.536$ Å (Si-220 monochromator in high resolution mode (bending 150) [6]) with an 8 mm pinhole mask in front of the detector. The maps collected on the TriCS diffractometer used a 40 step grid with a stepsize of 0.001 reciprocal lattice units (rlu). On HB-3A a 30 step grid with 0.002 rlu step size was used. In order to avoid confusion, the *HK*-values of the scans have been transformed to an orthogonal system using the *HH* direction as x and the $\bar{H}H$ direction as y. Additional data were taken with elastic measurements on the HB-1 spectrometer at HFIR and on CNCS at the SNS [9, 18]. These experiments were performed with the intent of measuring the magnetic excitation spectrum and therefore the sample consisted of ten co-aligned single crystals in (*HHL*) scattering geometry mounted on an aluminum sheet. The results from the inelastic measurements have been published in a separate publication [19]. On HB-1 the neutron wavelength of 2.46 Å from a PG-002 monochromator was used. The collimation was 48′–60′–60′–240′ with additional PG filters in the incident beam. The incident wavelength at CNCS was 2.60 Å.

Two data sets of nuclear Bragg reflections (40 and 65 reflections for orientations 1 and 2, respectively) were collected on TriCS for a scale factor determination at 300 and at 5 K with $\lambda = 1.178$ Å. These measurements proved the absence of reverse/obverse twinning [21] and confirmed the published nuclear structure [17].

3. Results

A diffraction map measured at $T = 2$ K on CNCS is shown in figure 1. With this pattern it is clear that the magnetic order is truly three-dimensional; in fact all measurements find the full width at half maximum (FWHM) in the L direction to be resolution limited (inset in figure 1). The correlation length is therefore larger than at least several hundred Å. This result clearly disagrees with the conclusions from the powder diffraction measurements [13, 14] (which were suggesting short range order along the L direction).

To identify the fundamental magnetic propagation vector, a detailed mapping of the magnetic reflections in the basal plane(s) has been performed at $T = 5$ K for both the TriCS and HB-3A datasets. Figure 2 gives an overview of the measured magnetic reflections and the related nuclear reflections to which they are satellite. The results are shown for the magnetic reflection with $L = 0$–2 around $(1/3, 1/3, L)$, and around $(-1/3, 2/3, L)$ in figure 3(a) and (b), respectively. The

[4] Kimura *et al* [3] defined the transition temperatures $T_N = T_{N2}$ and $T_{mf} = T_{N1}$. To be more precise we use T_N for the magnetic phase transition and T_{mf} for the transition to the multiferroic state.

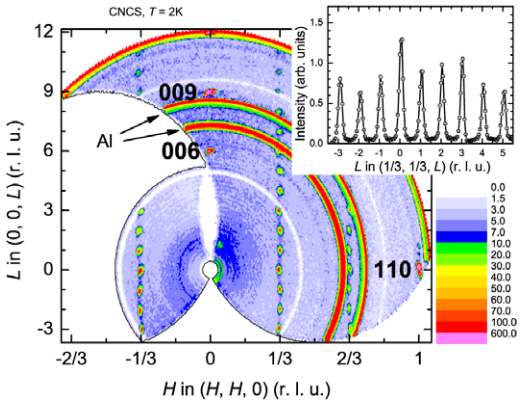

Figure 1. Reciprocal *HHL* map of $CuCrO_2$ measured on CNCS at $T = 2$ K. The nuclear (110), (006) and (009) Bragg peaks as well as the polycrystalline rings from the Al sample mount are marked. The unmarked reflections are magnetic. The inset in the upper right corner shows a section along $(1/3, 1/3, L)$. Axis values are in reciprocal lattice units (rlu).

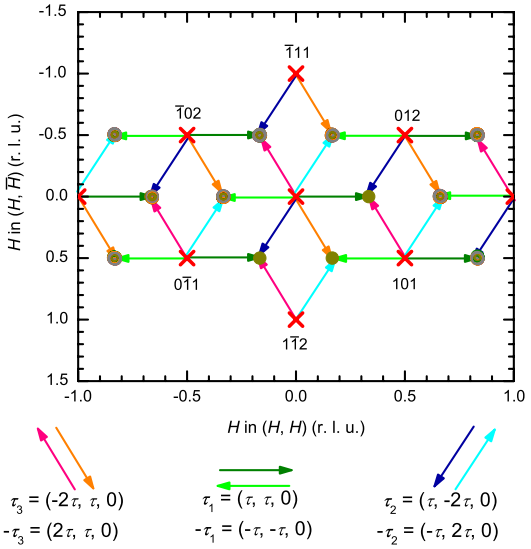

Figure 2. *HK*-projection of the magnetic reflections (circles) and their origin. The crosses mark the positions of the nuclear reflections. The star of the propagation vector τ is indicated by the different colored arrows.

figure shows the projection of the three observed reflections in the H, K-plane. The magnetic reflections are located around the commensurate 1/3 position which is also shown.

Based on our measurements, the magnetic structure of $CuCrO_2$ can be satisfactorily described with a pair of incommensurate propagation vectors $(\boldsymbol{\tau}_1, -\boldsymbol{\tau}_1)$ with $\boldsymbol{\tau}_1 = (\tau, \tau, 0)$ and $\tau = 0.3298(1)$. By symmetry, the star of the propagation vector consists of $\boldsymbol{\tau}_1 = (\tau, \tau, 0)$, $\boldsymbol{\tau}_2 = (\tau, -2\tau, 0)$ and $\boldsymbol{\tau}_3 = (-2\tau, \tau, 0)$ and their negative counterparts.

To confirm the magnetic structure a refinement of the two datasets measured at TriCS, collected with $\lambda = 1.178$ Å (139 reflections) and $\lambda = 2.32$ Å (197 reflections), has been performed using FullProf [20]. Three magnetic domains due to the three-fold axis have been taken into account.

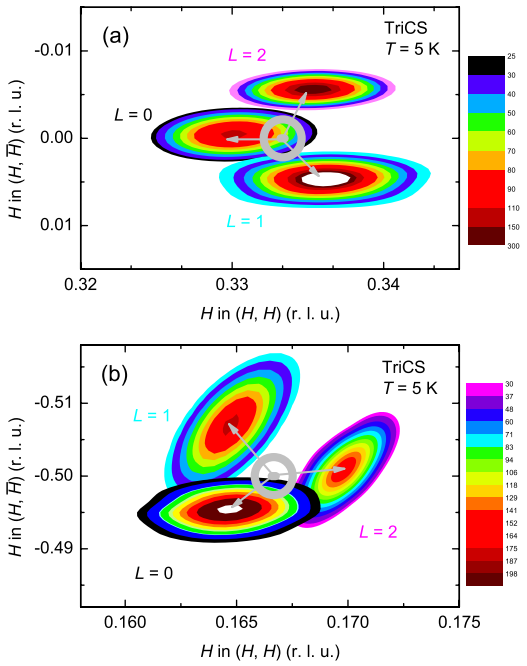

Figure 3. Upper panel: H, K-projection of the magnetic reflections around the $(1/3, 1/3, L)$ position (gray point) as measured on TriCS. Lower panel: magnetic reflections around the $(-1/3, 2/3, L)$ position. The color code of the intensity is shown on the right hand side and has been chosen to show the peaks to approximately two times the FWHM. The background is of the order of 5 in this arbitrary scale.

The following four models for the arrangement of magnetic moments were considered:

- amplitude modulated structure derived from the 'proper helix';
- 'cycloid 1' with moments rotating in the [110]–[001]-plane;
- 'cycloid 2' with moments rotating in the [110]–[1$\bar{1}$0]-plane;
- the 'proper helix' with moments rotating in the [1$\bar{1}$0]–[001]-plane as in [15].

The possibility of an elliptical envelope was allowed for the three last cases. Generally the magnetic moment $\mathbf{M}$ of the Cr^{3+} ion in the lth unit cell can be described by the generalized helix presentation

$$\mathbf{M}_l = \mathbf{M}_1 \cos(\boldsymbol{\tau} \cdot \mathbf{r}_l + \psi) + \mathbf{M}_2 \sin(\boldsymbol{\tau} \cdot \mathbf{r}_l + \psi),$$

where $\mathbf{M}_1$ and $\mathbf{M}_2$ are orthogonal base vectors determining the magnitude and direction of the generalized helix and ψ is the phase. $\boldsymbol{\tau}$ is the magnetic propagation vector and $\mathbf{r}_l$ is the vector to the magnetic ion in the lth unit cell.

The results for our refinement are listed in table 1. The cycloid models fit the experimental data poorly since they predict small intensities for the magnetic satellites along the wavevectors (i.e. $\boldsymbol{\tau}_1, \boldsymbol{\tau}_2, \boldsymbol{\tau}_3$).

In reality these intensities are large. This indicates that the magnetic moment is predominantly orthogonal to the wavevector. The amplitude modulated model agrees slightly

Table 1. Reliability factors for the magnetic structure at $T = 5$ K measured with $\lambda = 1.178$ Å. Four different prototype magnetic structures have been considered: amplitude modulated, cycloid 1 (*ab*-cycloid), cycloid 2 (110-*c*-cycloid) and proper helix. The refined parameters were the magnetic moment and the domain population.

Refined set of 139 magnetic reflections measured with 1.178 Å				
	Amplitude modulated	Cycloid 1	Cycloid 2	Proper helix
RF^2	35.0	43.1	35.1	28.0
RF^2w	38.1	44.7	38.1	30.6
RF	20.8	24.0	20.8	13.7
M_1 (μ_B)	$[1\bar{1}0]$ −0.1(6)	[110] 1(1)	[110] 0(8)	$[1\bar{1}0]$ 2.2(2)
M_2 (μ_B)	[001] 3.3(2)	$[1\bar{1}0]$ 3.2(4)	[001] 3.4(4)	[001] 2.8(2)
Domain population (%)	39(7):36(6):25(7)	39(9):40(9):22(9)	39(8):36(8):25(9)	37(2):37(2):26(3)

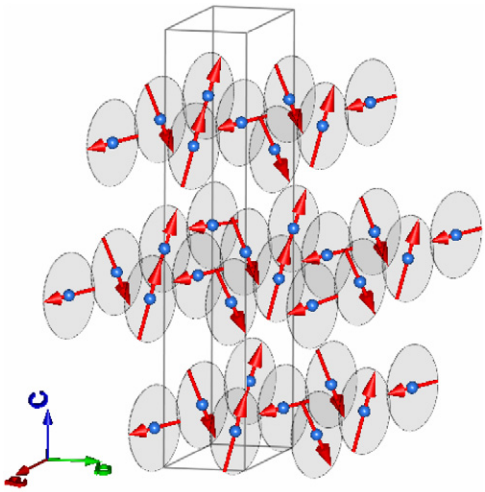

Figure 4. Real space representation of the magnetic structure of $CuCrO_2$. The chemical unit cell is outlined.

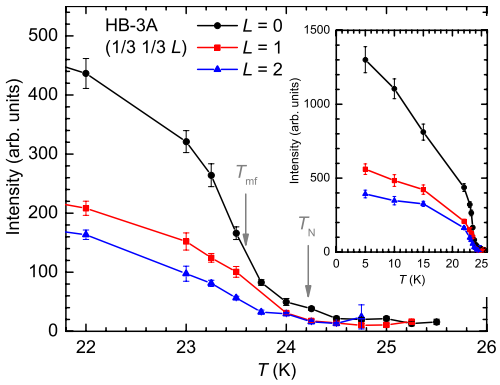

Figure 5. Intensity versus temperature plot for the magnetic reflections around $(1/3, 1/3, L)$ in the region from 22 to 26 K from measurements on HB-3A. The two transition temperatures T_N and T_{mf} are marked. The entire measured temperature range from 5 to 26 K is shown as an inset.

better with the data, but the agreement factors are larger than the ones obtained with the 'proper helix' model. Therefore, we agree with the powder diffraction results of Poienar *et al* [14] and polarized data of Soda *et al* [15] that the magnetic structure in $CuCrO_2$ is a proper helix. The statistically best fit is obtained for an elliptical helix with the moments averaged over all domains $\mathbf{M}_{[1\bar{1}0]} = 2.2(2)\ \mu_B$ and $\mathbf{M}_{[001]} = 2.8(2)\ \mu_B$. The data yield a different population for each domain. For the helix the obtained population is 37(2)%:37(2)%:26(3)%. In principle $\boldsymbol{\tau}_1$ and $-\boldsymbol{\tau}_1$ are not equivalent wavevectors and they might correspond to two different structures. Such a situation is, however, energetically not favored and we considered $\boldsymbol{\tau}_1$ and $-\boldsymbol{\tau}_1$ as generators to two chiral domains of the same structure. Figure 4 depicts the real space representation of the 'proper helix' model. The quantitative comparison between observed and calculated intensities can be found in table A.1 in the appendix.

We next discuss the temperature dependence of the magnetic structure. The magnetic intensity as shown in figure 5 decreases strongly with temperature above ∼23 K and would be in agreement with a critical temperature slightly below 24 K. However, the magnetic intensity above 24 K is still significant. Therefore the half-widths of the magnetic reflections were also analyzed along different lattice directions. Figure 6 shows three measurements for both the H, H and the L directions, below T_{mf}, between T_N and T_{mf}, and above T_N, respectively. Measured along the H, H direction the magnetic Bragg peak loses roughly a factor of four in intensity between 22 and 24 K but the width changes only slightly. At 26 K the magnetic intensity is then close to the background and the is intensity broadly smeared as expected above (but close to) the magnetic ordering temperature. Apparently T_{mf} is not a critical temperature along this direction. In the lower panel of figure 6 measurements along the L direction at the same temperatures are shown for comparison. Here, no sign of a Bragg peak can be seen in the intermediate temperature range, whereas along H, H there is still a peak, albeit small, at the same temperature. Along the L direction one finds *diffuse* magnetic scattering between T_N and T_{mf}, well above the instrumental background, indicative of a complete loss of the magnetic near neighbor correlations along this direction. Since the measurement uses energy analysis, the magnetic correlations can be considered static.

The picture becomes clear with an analysis of the temperature dependence of the widths of the Bragg peaks. This is shown in figure 7. The trend for the peak width along the *HH* direction is shown in the upper panel of figure 7. The width increases at increasing temperatures starting around 24 K. Above 25 K it then becomes difficult to fit a peak to the data. In contrast, the width along the L direction as shown

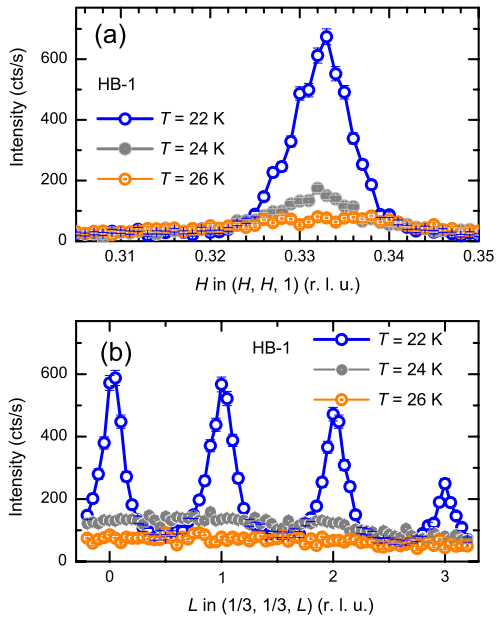

Figure 6. Magnetic intensities at three temperatures measured along the *HH* direction (a) and along the *L* direction (b) on HB-1.

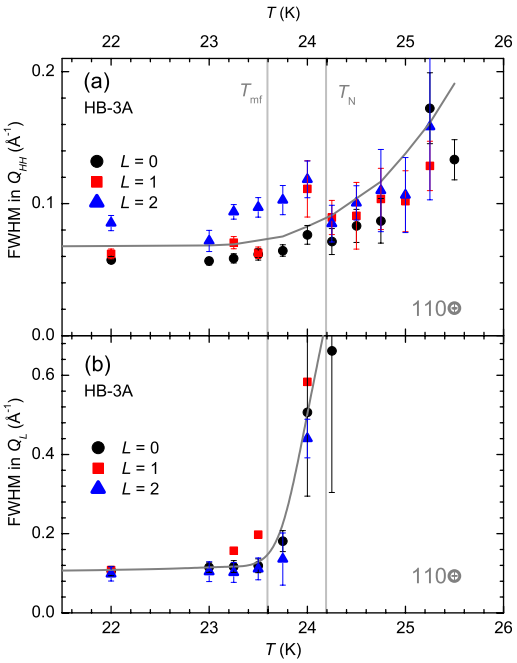

Figure 7. Temperature dependence of the FWHM of the magnetic satellites measured on HB-3A along (a) the *HH* direction and (b) the *L* direction in the temperature range from 22 to 26 K. The lines are guides to the eye. For comparison, the measured FWHM of the nuclear 110 reflection at room temperature in both directions is also shown. The vertical gray lines mark the transition temperatures T_N and T_{mf}. The width of the Bragg peaks along *L* diverges by approximately 1 K below the temperature at which it diverges along *HH*.

in the lower panel of the figure starts to significantly increase already above 23.6 K. At 24 K the fitted width is already as large as the distance between reciprocal lattice points.

To summarize, the picture that emerges is that $CuCrO_2$ enters a truly two-dimensional ordered state between T_N and T_{mf}, with well developed long range correlations in the H, K plane but a lack of correlation in the L direction. Only below T_{mf} is a three-dimensional ordering established.

4. Discussion

The new single crystal diffraction data and our analysis show that the low temperature magnetic ordering of $CuCrO_2$ is fully three-dimensional and can be described as an incommensurate proper helix propagating in the $[H, H, 0]$ direction. The moments are in the $[H, \bar{H}, L]$ plane. The envelope of the spiral is slightly elliptic. The magnetic propagation vector $\boldsymbol{\tau}$ is very close to the commensurate $(1/3, 1/3, 0)$ value. The commensurate case would correspond to the classic 120° magnetic ground state of the two-dimensional triangular lattice. The cause of the incommensurability of the propagation vector has been discussed earlier, and two different explanations have been proposed: either an in-plane lattice distortion [4, 5] or interlayer exchange interaction [22–25]. The latter is in better agreement with the occurrence of three-dimensional order, although the interlayer exchange is relatively small (0.02 meV) [19]. The maximum ordered moment in our model is 2.8(2) μ_B, which is close to the expected 3 μ_B for the Cr^{3+} ion and the reported values from the powder measurements [13, 14]. An additional uncertainty for the absolute moment value from the single crystal measurements comes from the non-equal domain distribution. A cycloidal spin structure can be excluded from our analysis, in accordance with the observation of multiferroicity in the low temperature phase and its explanation after Arima [7, 15, 26]. The 3D character of the low temperature ordering is in agreement with the interpretation of the earlier published specific heat data at the phase transition [14].

The multiferroic state of $CuCrO_2$ is entered without an apparent structural symmetry reduction or lattice distortion. Within the resolution of our experiments the upper limit for change of the lattice constants at the phase transition is 0.001 Å. However, evidence for in-plane distortions has been observed in high resolution x-ray diffraction measurements [5]. This is in agreement with the small structural distortion observed in the related $CuFeO_2$ system [12].

Why is $CuCrO_2$ not multiferroic between T_N and T_{mf}? According to the Arima model [26] the in-plane proper screw spiral will create a spontaneous polarization even without the observed three-dimensional order. The propagation vector in the narrow phase is the same as in the multiferroic phase and it will be argued in the following why the magnetic structure in the intermediate phase is most likely an in-plane proper screw but without interlayer order. In the light of the two-dimensional nature this narrow phase has been discussed as a possible collinear state [2]. However, it is unlikely that the narrow temperature phase has a collinear structure. It has been shown theoretically [27] that the collinear state is energetically not favored, but might be entered at high (>90 T) magnetic fields [28]. Also, a collinear state with

three sublattices would have a net ferromagnetic moment (which is not observed). A re-ordering from collinear to helical state is expected to feature a large response in the temperature dependent susceptibility (which is not observed). Similarly, an amplitude modulated magnetic structure on a three sublattice without a ferromagnetic net moment would undergo a discontinuous phase transition to a spiral state.

Our results show that the propagation vector remains the same in both phases. In combination with the absence of a net ferromagnetic component and the continuous course of the susceptibility through the transition at T_{mf} this indicates that spirals already form at T_N. In the L direction uncorrelated spirals then order through ferromagnetic interlayer exchange to a full three-dimensional order at T_{mf}. The question why $CuCrO_2$ is not multiferroic between T_N and T_{mf} cannot be answered with the results from the diffraction experiment alone, since in the picture of the uncorrelated spirals the spontaneous polarization could be averaged to zero. A possible experiment to clarify this question is neutron diffraction with an applied electric field in this narrow phase.

Acknowledgments

We acknowledge the technical and scientific support from the staff at SNS, HFIR, and PSI. This work was partly performed at SINQ, Paul Scherrer Institute, Villigen, Switzerland. This research was sponsored by the Division of Materials Sciences and Engineering of the US Department of Energy. Research at Oak Ridge National Laboratory's Spallation Neutron Source was supported by the Scientific User Facilities Division, Office of Basic Energy Sciences, US Department of Energy. The work in Minsk was supported in part by the Belarusian Fund for Basic Scientific Research, grant No F10R-154.

Appendix

Table A.1. The intensities of the 139 measured reflections at $T = 5$ K ($\lambda = 1.178$ Å) compared with the calculated intensities for the 'proper helix' model.

h	k	l	I_{obs}	I_{calc}	$\lvert I_{obs} - I_{calc}\rvert$	h	k	l	I_{obs}	I_{calc}	$\lvert I_{obs} - I_{calc}\rvert$
−1	2	0	13.1	6.8371	6.2629	−1	1	7	5.74	5.7226	0.0174
1	−1	−7	6.88	5.7226	1.1574	−1	1	7	5.89	5.7226	0.1674
0	2	−2	10.38	8.3391	2.0409	2	0	2	8.46	8.3392	0.1208
−2	0	−2	9.29	8.3392	0.9508	−2	1	3	6.98	5.7782	1.2018
−1	2	−3	4.54	5.7782	1.2382	−1	2	3	5.89	5.7782	0.1118
−2	1	−3	3.74	5.7782	2.0382	0	−1	10	4.24	3.9125	0.3275
0	1	−10	5.06	3.9125	1.1475	1	0	10	4.36	3.9125	0.4475
−1	0	−10	3.95	3.9125	0.0375	0	1	−4	7.66	7.6383	0.0217
1	0	4	8.65	7.6383	1.0117	−1	0	−4	7.6	7.6383	0.0383
−2	0	4	5.26	6.5873	1.3273	2	0	−4	5.23	6.5873	1.3573
0	2	4	5.2	6.5873	1.3873	−1	1	−8	3.17	4.3896	1.2196
1	−1	8	4.24	4.3896	0.1496	−1	1	−8	3.74	4.3896	0.6496
−1	0	5	4.28	6.4112	2.1312	1	0	−5	5.4	6.4112	1.0112
0	1	5	4.12	6.4112	2.2912	0	2	−5	5.59	5.5569	0.0331
2	0	5	7.7	5.5569	2.1431	−2	0	−5	6.59	5.5569	1.0331
−1	0	11	4.09	2.817	1.273	1	0	−11	3.91	2.817	1.093
0	1	11	2.8	2.817	0.017	0	−1	−11	2.54	2.817	0.277
−2	1	6	3.26	3.5908	0.3308	−1	2	−6	3.11	3.5908	0.4808
−1	2	6	3.49	3.5908	0.1008	2	−1	6	1.62	3.5908	1.9708
−2	1	−6	3.74	3.5908	0.1492	−1	−1	9	4.72	4.0286	0.6914
1	1	−9	3.49	4.0286	0.5386	1	1	9	5.26	4.0286	1.2314
2	−1	0	45.12	27.9165	17.2035	−2	1	0	45.73	27.9165	17.8135
2	−1	0	45.12	27.9165	17.2035	−2	1	0	45.73	27.9165	17.8135
−1	−1	0	15.4	12.0966	3.3034	1	1	0	14.71	12.0966	2.6134
1	−2	0	12.85	10.1287	2.7213	−1	2	0	13.24	10.1287	3.1113
−1	−1	0	7.29	4.1887	3.1013	1	1	0	9.05	4.1887	4.8613
1	−2	0	7.66	2.7403	4.9197	0	1	−7	6.42	7.3848	0.9648
−1	0	2	11.78	14.2513	2.4713	1	0	−2	11.5	14.2513	2.7513
0	−1	7	7.78	9.6636	1.8836	0	1	−7	8.3	9.6636	1.3636
1	1	−3	7.69	10.1203	2.4303	1	1	3	6.53	10.1203	3.5903
−1	2	−3	9.76	8.5424	1.2176	−1	2	3	6.95	8.5424	1.5924
1	0	10	6.38	5.8874	0.4926	−1	0	−10	6.04	5.8874	0.1526
−1	1	10	6.35	5.3961	0.9539	−2	0	4	6.84	10.9539	4.1139
2	0	−4	7.74	10.9539	3.2139	−1	1	4	10.72	8.9407	1.7793
−2	2	−4	6.13	7.4791	1.3491	1	0	4	11.06	11.1608	0.1008
−1	0	−4	10.98	11.1608	0.1808	0	1	8	5.28	5.7154	0.4354
0	1	8	5.81	7.3099	1.4999	2	0	5	8.3	9.1917	0.8917
−2	0	−5	8.33	9.1917	0.8617	−2	2	5	9.59	6.367	3.223
1	−1	5	5.68	7.5568	1.8768	−1	1	−5	5.54	7.5568	2.0168
−1	0	5	6.54	9.3597	2.8197	1	0	−5	5.58	9.3597	3.7797

Table A.1. (Continued.)

h	k	l	I_{obs}	I_{calc}	$\lvert I_{obs} - I_{calc}\rvert$	h	k	l	I_{obs}	I_{calc}	$\lvert I_{obs} - I_{calc}\rvert$
−1	0	11	4.14	4.2058	0.0658	1	0	−11	4.75	4.2058	0.5442
1	−1	11	5	3.9022	1.0978	−1	1	−11	4.85	3.9022	0.9478
1	1	−6	4.92	6.1313	1.2113	1	1	6	2.69	6.1313	3.4413
−2	1	9	4.4	5.3651	0.9651	2	−1	−9	6.22	5.3651	0.8549
2	−1	9	8.62	5.3651	3.2549	−2	1	−9	4.18	5.3651	1.1851
−1	2	−6	5.15	5.2815	0.1315	−1	2	6	3.37	5.2815	1.9115
−2	0	7	3.25	5.8968	2.6468	0	0	0	80.57	60.254	20.316
0	0	0	80.06	60.254	19.806	1	0	7	6.7	7.4263	0.7263
−1	0	−7	6.53	7.4263	0.8963	0	1	2	11.06	14.3314	3.2714
1	0	7	5.04	9.7179	4.6779	−1	−1	3	6.49	10.1772	3.6872
1	1	−3	5.62	10.1772	4.5572	1	1	3	7.09	10.1772	3.0872
−1	−1	−3	8.28	10.1772	1.8972	−2	1	3	5.77	8.5905	2.8205
2	−1	−3	4.94	8.5905	3.6505	2	−1	3	7.21	8.5905	1.3805
−2	1	−3	7.02	8.5905	1.5705	0	−1	10	6.04	5.9204	0.1196
0	1	−10	6.35	5.9204	0.4296	−1	1	10	6.7	5.4264	1.2736
1	−1	−10	5.69	5.4264	0.2636	0	2	4	5.54	11.0155	5.4755
−1	1	4	10.44	8.991	1.449	2	−2	4	5.45	7.5211	2.0711
−2	2	−4	4.32	7.5211	3.2011	0	1	−4	11.72	11.2235	0.4965
−1	0	8	4.82	5.7475	0.9275	1	0	−8	5.14	5.7475	0.6075
−1	0	8	4.49	7.351	2.861	1	0	−8	5.1	7.351	2.251
0	2	−5	6.28	9.2434	2.9634	−2	2	5	5.69	6.4027	0.7127
−1	1	−5	3.82	7.5992	3.7792	0	1	5	5.15	9.4123	4.2623
0	1	11	6.6	4.2294	2.3706	0	−1	−11	4.81	4.2294	0.5806
1	−1	11	3.76	3.9241	0.1641	−1	1	−11	3.22	3.9241	0.7041
−1	−1	6	3.19	6.1658	2.9758	1	1	−6	3.25	6.1658	2.9158
1	1	6	5.14	6.1658	1.0258	−1	−1	−6	5.4	6.1658	0.7658
1	−2	9	9.47	5.3953	4.0747	−1	2	−9	7.09	5.3953	1.6947
−1	2	9	5.71	5.3953	0.3147	−2	1	6	2.63	5.3112	2.6812
2	−1	−6	3.3	5.3112	2.0112	2	−1	6	6.11	5.3112	0.7988
−2	1	−6	5.14	5.3112	0.1712						

References

[1] Cheong S-W and Mostovoy M 2007 Multiferroics: a magnetic twist for ferroelectricity *Nature Mater.* **6** 13

[2] Kimura K, Nakamura H, Ohgushi K and Kimura T 2008 Magnetoelectric control of spin-chiral ferroelectric domains in a triangular lattice antiferromagnet *Phys. Rev.* B **78** 140401

[3] Kimura K, Nakamura H, Kimura S, Hagiwara M and Kimura T 2009 Tuning ferroelectric polarization reversal by electric and magnetic fields in $CuCrO_2$ *Phys. Rev. Lett.* **103** 107201

[4] Yamaguchi H, Ohtomo S, Kimura S, Hagiwara M, Kimura K, Kimura T, Okuda T and Kindo K 2010 Spiral-plane flop probed by esr in the multiferroic triangular-lattice antiferromagnet $CuCrO_2$ *Phys. Rev.* B **81** 033104

[5] Kimura K, Otani T, Nakamura H, Wakabayashi Y and Kimura T 2009 Lattice distortion coupled with magnetic ordering in a triangular lattice antiferromagnet $CuCrO_2$ *J. Phys. Soc. Japan* **78** 113710

[6] Chakoumakos B C, Cao H, Ye F, Stoica A D, Popovici M, Sundaram M, Zhou W, Steve Hicks J, Lynn G W and Riedel R A 2011 Four-circle single-crystal neutron diffractometer at the high flux isotope reactor *J. Appl. Crystallogr.* **44** 655–8

[7] Soda M, Kimura K, Kimura T, Matsuura M and Hirota K 2009 Electric control of spin helicity in multiferroic triangular lattice antiferromagnet $CuCrO_2$ with proper-screw order *J. Phys. Soc. Japan* **78** 124703

[8] Schefer J, Könnecke M, Murasik A, Czopnik A, Strässle Th, Keller P and Schlumpf N 2000 Single-crystal diffraction instrument trics at sinq *Physica* B **276–278** 168–9

[9] Mason T E *et al* 2006 The spallation neutron source in Oak Ridge: a powerful tool for materials research *Physica* B **385/386** 955–60

[10] Petrenko O A, Balakrishnan G, Lees M R, Paul D McK and Hoser A 2000 High-magnetic-field behavior of the triangular-lattice antiferromagnet $CuFeO_2$ *Phys. Rev.* B **62** 8983

[11] Kimura T, Lashley J C and Ramirez A P 2006 Inversion-symmetry breaking in the noncollinear magnetic phase of the triangular-lattice antiferromagnet $CuFeO_2$ *Phys. Rev.* B **73** 220401

[12] Ye F, Ren Y, Huang Q, Fernandez-Baca J A, Dai P, Lynn J W and Kimura T 2006 Spontaneous spin-lattice coupling in the geometrically frustrated triangular lattice antiferromagnet $CuFeO_2$ *Phys. Rev.* B **73** 220404

[13] Kadowaki H, Kikuchi H and Ajiro Y 1990 Neutron powder diffraction study of the two-dimensional triangular lattice antiferromagnet $CuCrO_2$ *J. Phys.: Condens. Matter* **2** 4485

[14] Poienar M, Damay F, Martin C, Hardy V, Maignan A and André G 2009 Structural and magnetic properties of $CuCr_{1-x}Mg_xO_2$ by neutron powder diffraction *Phys. Rev.* B **79** 014412

[15] Soda M, Kimura K, Kimura T and Hirota K 2010 Domain rearrangement and spin-spiral-plane flop as sources of magnetoelectric effects in delafossite $CuCrO_2$ *Phys. Rev.* B **81** 100406(R)

[16] Crottaz O, Kubel F and Schmid H 1996 Preparation of trigonal and hexagonal cuprous chromite and phase transition study based on single crystal structure data *J. Solid State Chem.* **122** 247–50

[17] Crottaz O and Kubel F 1996 Crystal structure of copper(i) chromium(iii) oxide, 3r-$CuCrO_2$ *Z. Kristallogr.* **211** 482–2

[18] Ehlers G, Podlesnyak A A, Niedziela J L, Iverson E B and Sokol P E 2011 The new cold neutron chopper spectrometer at the spallation neutron source: design and performance *Rev. Sci. Instrum.* **82** 085108
[19] Frontzek M, Haraldsen J T, Podlesnyak A, Matsuda M, Christianson A D, Fishman R S, Sefat A S, Qiu Y, Copley J R D, Barilo S, Shiryaev S V and Ehlers G 2011 Magnetic excitations in the geometric frustrated multiferroic $CuCrO_2$ *Phys. Rev.* B **84** 094448
[20] Rodríguez-Carvajal J 1993 Recent advances in magnetic structure determination by neutron powder diffraction *Physica* B **192** 55–69
[21] Herbst-Irmer R and Sheldrick G M 2002 Refinement of obverse/reverse twins *Acta Crystallogr.* B **58** 477–81
[22] Rastelli E and Tassi A 1986 The rhombohedral Heisenberg antiferromagnet: infinite degeneracy of the ground state and magnetic properties of solid oxygen *J. Phys. C: Solid State Phys.* **19** L423
[23] Rastelli E and Tassi A 1987 Order produced by quantum disorder in the Heisenberg rhombohedral antiferromagnet *J. Phys. C: Solid State Phys.* **20** L303
[24] Rastelli E and Tassi A 1988 Collinear and helical phases of the monoclinic and rhombohedral antiferromagnet. Application to the α- and β-phases of solid oxygen *J. Phys. C: Solid State Phys.* **21** 1003
[25] Kadowaki H, Takei H and Motoya K 1995 Double-q 120° structure in the Heisenberg antiferromagnet on rhombohedrally stacked triangular lattice $LiCrO_2$ *J. Phys.: Condens. Matter* **7** 6869
[26] Arima T 2007 Ferroelectricity induced by proper-screw type magnetic order *J. Phys. Soc. Japan* **76** 073702
[27] Fishman R S 2011 Phase diagram of a geometrically frustrated triangular-lattice antiferromagnet in a magnetic field *Phys. Rev. Lett.* **106** 037206
[28] Fishman R S 2011 Phase diagram of $CuCrO_2$ in a magnetic field *J. Phys.: Condens. Matter* **23** 366002